Available online at www.sciencedirect.com
ScienceDirect
ELSEVIER
ISPRS Journal of Photogrammetry & Remote Sensing 62 (2007) 309–324
PHOTOGRAMMETRY & REMOTE SENSING
www.elsevier.com/locate/isprsjprs

Estimation of vegetation parameter for modeling soil erosion using linear Spectral Mixture Analysis of Landsat ETM data

Alejandro M. de Asis, Kenji Omasa *

Graduate School of Agricultural and Life Sciences, The University of Tokyo, Yayoi 1-1-1, Bunkyo-ku, Tokyo, 113-8657, Japan

Received 7 November 2006; received in revised form 16 May 2007; accepted 18 May 2007
Available online 5 July 2007

Abstract

Soil conservation planning often requires estimates of soil erosion at a catchment or regional scale. Predictive models such as Universal Soil Loss Equation (USLE) and its subsequent Revised Universal Soil Loss Equation (RUSLE) are useful tools to generate the quantitative estimates necessary for designing sound conservation measures. However, large-scale soil erosion model-factor parameterization and quantification is difficult due to the costs, labor and time involved. Among the soil erosion parameters, the vegetative cover or *C* factor has been one of the most difficult to estimate over broad geographic areas. The *C* factor represents the effects of vegetation canopy and ground covers in reducing soil loss. Traditional methods for the extraction of vegetation information from remote sensing data such as classification techniques and vegetation indices were found to be inaccurate. Thus, this study presents a new approach based on Spectral Mixture Analysis (SMA) of Landsat ETM data to map the *C* factor for use in the modeling of soil erosion. A desirable feature of SMA is that it estimates the fractional abundance of ground cover and bare soils simultaneously, which is appropriate for soil erosion analysis. Hence, we estimated the *C* factor by utilizing the results of SMA on a pixel-by-pixel basis. We specifically used a linear SMA (LSMA) model and performed a minimum noise fraction (MNF) transformation and pixel purity index (PPI) on Landsat ETM image to derive the proportion of ground cover (vegetation and non-photosynthetic materials) and bare soil within a pixel. The end-members were selected based on the purest pixels found using PPI with reference to very high-resolution QuickBird image and actual field data. Results showed that the *C* factor value estimated using LSMA correlated strongly with the values measured in the field. The correlation coefficient (r) obtained was 0.94. A comparative analysis between NDVI- and LSMA-derived *C* factors also proved that the latter produced a more detailed spatial variability, as well as generated more accurate erosion estimates when used as input to RUSLE model. The QuickBird image coupled with field data was used in the validation of results.

Keywords: Spectral Mixture Analysis; NDVI; Landsat ETM; Vegetation analysis; Soil erosion

1. Introduction

Vegetation cover is one of the most crucial factors in reducing soil erosion. In general, as the protective canopy of land cover increases, soil erosion decreases (Elwell and Stocking, 1976). Vegetation reduces soil erosion by: protecting the soil against the action of falling raindrops, increasing the degree of infiltration of water into the soil, reducing the speed of the surface run-off, binding the soil mechanically, maintaining the roughness of the soil surface, and improving the physical; chemical and biological properties of the soil (Baver, 1956).

* Corresponding author. Tel.: +81 3 5841 5340; fax: +81 3 5841 8175.
E-mail address: aomasa@mail.ecc.u-tokyo.ac.jp (K. Omasa).

0924-2716/$ - see front matter © 2007 International Society for Photogrammetry and Remote Sensing, Inc. (ISPRS). Published by Elsevier B.V. All rights reserved.
doi:10.1016/j.isprsjprs.2007.05.013

In soil erosion models such as the Universal Soil Loss Equation (USLE) (Wischmeier and Smith, 1978) and its subsequent Revised Universal Soil Loss Equation (RUSLE) (Renard et al., 1997), the effect of vegetation is accounted for in the vegetation cover factor or *C* factor. In both models, the average soil erosion per year is computed from the product of six factors, namely: rainfall erosivity (*R*), soil erodibility (*K*), slope length (*L*), slope steepness (*S*), vegetation cover (*C*), and support practice factor (*P*). From the standpoint of soil conservation planning, the vegetation cover factor is the most essential because the land-use changes that are meant to reduce soil erosion are represented by this factor.

The *C* factor has been one of the most difficult USLE or RUSLE coefficients to estimate over broad geographic areas. Traditionally, spatial estimates of vegetation cover, or *C* factor, have been done by simply assigning *C* factor values from literature or field data into a classified land cover map (cover classification method) (Folly et al., 1996; Juergens and Fander, 1993; Morgan, 1995). This method, however, resulted in *C* factor estimates that are constant for relatively large areas, and do not adequately reflect the variation in vegetation that exists within large geographic areas (Wang et al., 2002). Errors in classification are also introduced in the *C* factor map. To increase the spatial variability and decrease the influence of classification errors, direct linear regression has been performed between image bands or ratios and *C* values determined in the field (Cihlar, 1987; Stephens and Cihlar, 1982). Gertner et al. (2002) and Wang et al. (2002, 2003) used joint sequential co-simulation with Landsat TM images for mapping the *C* factor from point values. However, this method is costly and obtaining the appropriate number of sampling points for interpolation is rather difficult.

Vegetation indices such as Normalized Difference Vegetation Index (NDVI) have also been explored for mapping the *C* factor by relating it directly to USLE and RUSLE-*C* factor by regression analysis. However, satellite image-driven vegetation indices were found to have low correlation with the *C* factor (De Jong, 1994; Tweddales et al., 2000). De Jong (1994) explained that the low correlation is due to the sensitivity of vegetation to vitality, as the condition of the vegetation is not always related to its soil protective function. Despite these issues, the NDVI is one of the commonly used methods to determine the *C* factor using remote sensing for soil erosion assessment over regional or large geographic area (e.g. Cartagena, 2004; De Jong et al., 1999; Hazarika and Honda, 2001; Lin et al., 2002, 2006; Lu et al., 2003; Najmoddini, 2003; Symeonakis and Drake, 2004; Van der Knijff et al., 2002).

Other than the USLE and RUSLE, the *C* factor is also applied to other erosion models such as the Morgan and Finney method (Morgan et al., 1984), ANSWERS (Beasley et al., 1980), WEPP (NSERL, 1995), SEMMED (De Jong and Riezebos, 1997) and PCARES (Paningbatan, 2001). Thus, it is important to improve the ways in which the *C* factor is estimated using remote sensing. A reliable vegetation cover factor estimate is essential for accurate identification and estimation of soil erosion, which in turn, is needed for sound conservation planning.

In this paper, we present a new technique based on linear Spectral Mixture Analysis (LSMA) in assessing vegetation and soil status, and compare its potential for deriving and mapping *C* factor values with the commonly used NDVI method. LSMA is a sub-pixel classification technique, which assumes that the spectrum measured by a sensor is a linear combination of the spectra of components within the instantaneous field of view (Gilabert et al., 2000; Roberts et al., 1993). A desirable feature of the LSMA model is that it can estimate the fractional abundance of green vegetation and soils simultaneously, which is appropriate for purposes that require both information at the same instant such as in the case of erosion analysis (Paringit and Nadaoka, 2003). The LSMA was also found useful in estimating the percentage of ground cover such as crop residues, which also play a major role in controlling soil erosion (Arsenault and Bonn, 2005; Biard and Baret, 1997). Hence, in this study, we attempted to estimate the *C* factor as a function of the fractional abundance of bare soil and ground cover (both green vegetation and non-photosynthetic materials) in a given pixel of a Landsat ETM. A comparative analysis of soil erosion (using the RUSLE model) between NDVI- and LSMA-derived *C* factors as inputs to the soil erosion model was also conducted to determine its validity for the estimation of soil erosion.

2. Methods

2.1. Study area

The study area is the Lamesa watershed located in the northernmost part of Metro Manila, Philippines between 14.70 to 14.77 N latitude and 120.98 to 121.12 E longitude (Fig. 1). This is a watershed reservation covering an area of about 2700 ha and consists mainly of evergreen secondary forests and grasslands. The area experienced high deforestation rates in the past, which resulted in the conversion of a large natural forest into grassland. Cultivated lands and abandoned slash and

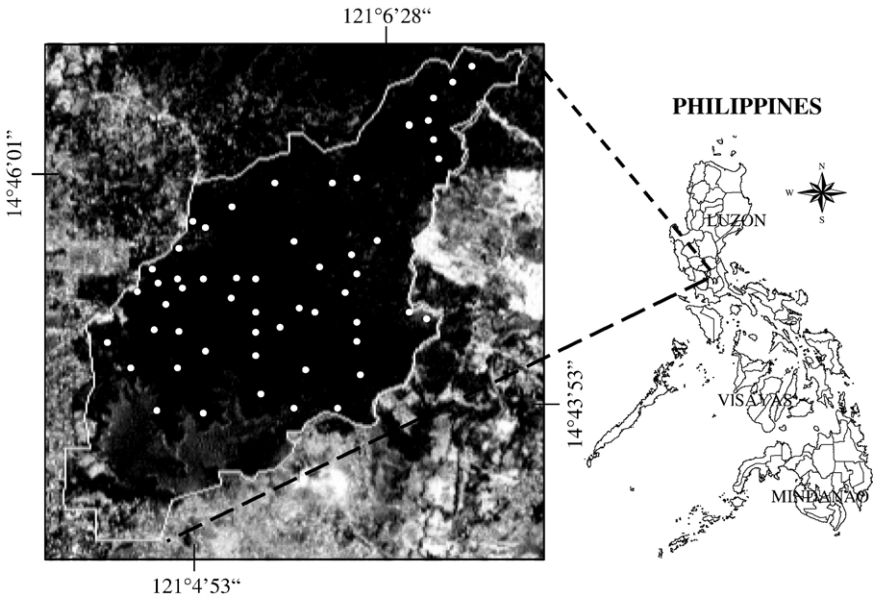

Fig. 1. Geographic location of the Lamesa watershed. The dots show the relative locations of 53 sampling sites in the study area.

burn areas can also be found in patches. These areas are characterized by very little vegetation cover, which usually dries up during the dry season. Fortunately, various efforts are now being undertaken to rehabilitate and preserve the watershed. Soil conservation is of significant concern because this area supports a critically important water resource for Metro Manila.

The topography of the Lamesa watershed is characterized by gently undulating terrain. Elevations vary from 64 m to 248 m above mean sea level. Its climate is dominated by distinct rainy and dry seasons. The study area is relatively dry from December to April and wet from May to November with maximum monthly precipitation ranging from 488 mm to 1469 mm. Mean annual precipitation is 2069 mm. It is hot from March to May, with temperature usually reaching to around 35 °C. Average temperatures rarely drop below 27 °C.

2.2. Satellite data and image pre-processing

A Landsat ETM+scene (path 116, row 50) taken on April 24, 2004 was acquired and analyzed by this study. Landsat ETM data was used because it is inexpensive, with high monitoring frequency and covers large areas appropriate for developing soil conservation planning for a large geographic area. The Landsat ETM has a temporal revisit time of 16 days and a spatial resolution of 30 m with six visible/near infrared bands and one thermal band. In this study, the digital number (DN) of ETM bands 1–5 and 7 recorded in 8 bits were converted to exo-atmospheric reflectance units as described in the Landsat 7 Users Handbook (http://ltpwww.gsfc.nasa.gov/IAS/ handbook/handbook_toc.html). This involved a conversion from DN to radiance, which took advantage of the LMIN and LMAX (spectral radiances for each band at digital numbers 0 or 1 and 255) values provided in the image metafile and then converting the radiance values to reflectance using:

$$\rho_\lambda = \frac{\pi \cdot L_\lambda \cdot d^2}{\mathrm{ESUN}_\lambda \cdot \sin(\theta)} \quad (1)$$

where; L and ρ are spectral radiance and reflectance, respectively. The subscript λ refers to spectral band λ, ESUN_λ is the solar irradiance, θ is sun elevation and d is sun–earth distance. The most current exo-atmospheric solar irradiance values for the Landsat ETM were used in the radiance to reflectance conversion. The conversion from DN to reflectance value can substantially improve the quality of image (Huang et al., 2002). The image was then geometrically rectified using ground control points to accurately link it to ground reference data. The control points were taken from topographic maps, which were further validated using coordinates measured with a Differential Global Positioning System (DGPS) to ensure matching of ground data (i.e. sampling sites) with the image. A nearest neighborhood

algorithm was used in the image resampling, which yielded a root mean square error of 0.37 pixels. The Landsat scene was geo-referenced to Universal Transverse Mercator Projection (WGS 84) and was reduced to size covering only the study area as shown in Fig. 1.

Another image used in the study was a QuickBird multispectral image taken on April 25, 2004. The QuickBird image has four discrete non-overlapping bands with resolution of 2.44 m and is recorded in 11 bits. Because of its high resolution, it is possible to identify the location of erosion areas. Hence, coupled with field data, this image was used to validate the results of erosion modeling.

2.3. Field data collection

Fieldwork was conducted on several occasions during the same month the images were taken. The fieldwork basically involved the measurement of different parameters for the *C* factor estimation. Normally, the *C* factor is evaluated from long-term experiments where soil loss is measured from field plots. However, in the absence of long-term experimental data, it is possible to estimate the *C* factor by using sub-factors, as advocated by Wischmeier and Smith (1978) who identified three major sub-factors instrumental to the vegetation's effectiveness in limiting soil erosion. These are: (1) canopy cover, (2) ground cover, and (3) below ground surface effects (i.e. effects of roots). Dissmeyer and Foster (1981) modified and made additional sub-factors to adapt it to forest conditions. These include the percentage of ground cover (amount of soil surface covered by materials such as litter, dried leaves, branches, logs, rocks or gravel), percentage of bare soil, percentage of canopy cover, soil reconsolidation, organic matter content, fine roots, residual binding effect and onsite storage of water. In this study, we used the Dissmeyer and Foster (1981) method to determine the *C* factor in the field.

Prior to the fieldwork, a detailed examination of False Color Composite of a Landsat ETM image and a topographic map of the study area was conducted to get an overall view and to systematically identify and select sampling areas for the *C* factor evaluation. A DGPS was used to locate and define the sampling areas. Using the DGPS, the Landsat ETM pixels that correspond to a 60×60-meter area on the ground were identified (covering 4 pixels of Landsat ETM). The DGPS consisted of two hand-held Magellan ProMark X-CM GPS receivers: one base receiver sited at a known position, and a rover receiver used in the field. The two receivers were set to collect data simultaneously, and common errors such as atmospheric disturbances have been eliminated. The distance error of the DGPS is less than 2 m.

A total of fifty-three (53) sampling sites were located and established in the study area (refer to Fig. 1). At each site, the percentage of canopy cover, ground cover, and bare soil were estimated using the line-point intercept sampling method (Morrison et al., 1993). Measurements were taken along 60 m long transects placed across the study plot. Pin flags were lowered at 60 cm intervals along the entire length of the transect. At each point, the types of cover were recorded and the percentages of each variable were calculated. The overstory canopy of trees at least 3 m tall were estimated using a densiometer method (Ganey and Block, 1994). Other data evaluated at each sampling site were the percentage of fine roots in bare soil areas, the presence of steps, onsite water storage, and organic matter content. Soil samples were collected to determine the organic matter content of the soil. The *C* factor was then estimated for each site by using the field data following the approach described by Dissmeyer and Foster (1981).

2.4. Linear Spectral Mixture Analysis

Pixels containing mixed spectral information about the objects under study are commonly found in remotely sensed data. This is due to the limitations of the spatial resolution of the satellite instruments (such as TM, ETM+, HRV of SPOT, etc.) and the heterogeneity of features on the ground. The mixture spectra are generated when the pixel covers more than one land cover class.

Spectral Mixture Analysis (SMA) has often been implemented to deal with the problem of mixed pixels. The linear spectral unmixing model (Adams et al., 1986; Settle and Drake, 1993; Van der Meer, 1995) is by far the most common type of SMA, and although theoretically imperfect due to the omission of the effect of multiple scattering between cover types (Roberts et al., 1993; Myneni et al., 1995), the errors associated with the linear assumptions have been found to be relatively minor (Kerdiles and Grondona, 1995). Linear SMA models have also been proven to be reasonably effective in estimating end-member fractions (Adams et al., 1986; Elmore et al., 2000; Small, 2003; Smith et al., 1990) and widely used due to their simplicity, reasonable effectiveness and interpretability (Xiao and Moody, 2005).

An important assumption of the LSMA is that the spectral signature of a given pixel is the linear, proportion-weighted combination of the end-member

spectra (Smith et al., 1990). An end-member is a pure surface material or land cover type that is assumed to have a unique spectral signature (referred to as the end-member signature). Mathematically, the general form of the LSMA is:

$$R_i = \sum_{j=1}^{n} F_j \times R_{Eij} + \varepsilon_i \quad \text{and} \qquad (2)$$

$$\sum_{j=1}^{n} F_j = 1; 0 \leq F_j \leq 1$$

where i is the number of spectral bands used, $j=1,\ldots, n$ (number of end-members), R_i is the spectral reflectance of the mixed pixel in band i, F_j is the fraction of the pixel area covered by the end-member j, R_{Eij} denotes the reflectance of the end-member j in band i, and ε_i is the residual error in band i. The residual error ε is the difference between the measured and modeled reflectance in each band. Residuals over all bands for each pixel in the image can be averaged to give a root mean square error (RMSE), which is useful in assessing the validity of selected end-members. A small RMSE for instance, is an indication that end-members were properly selected and the number of selected end-members is sufficient.

In addition, two constraints were maintained in the solution of F_j values. These are: the fractions across all end-members sum to one, and each end-member fraction is in the range 0 to 1. Input for the model is the spectral reflectance (R_i) and the pure spectra of components in the pixel (R_{Eij}). Using this known parameter in the equation will give the areal proportion for end-members. A unique solution is possible as long as the number of end-members is equal to the number of spectral bands used plus one.

The selection of suitable end-members is the most critical step in the development of high quality fraction images. There are different methods for selecting end-members from the image (e.g. Boardman et al., 1995; Oki et al., 2002; Small, 2003; Tompkins et al., 1997; Wu and Murray, 2003) including the use of two-dimensional feature space plots (Peterson and Stow, 2003) and the identification of pure pixels with reference to field data (Shoshany and Svoray, 2002). In this study, a combination of automatic and supervised end-member selections was performed on the Landsat ETM image. The minimum noise fraction (MNF) algorithm was applied to the reflectance image in which the MNF-transformed data were used as input to determine the most spectrally pure pixels (i.e. candidate end-members) in the image. The MNF is essentially a two cascaded principal component transformation that first computes the estimated noise covariance matrix to decorrelate and rescale the noise in the data and then performs a standard principal component transform of the noise-whitened data (Garcia and Ustin, 2001). In the MNF transform, the noise is separated from the data by using only the coherent portions, thus improving spectral processing results. Previous studies have shown that the use of the MNF transform can improve the quality of fraction images (Van der Meer and De Jong, 2000) through decorrelation. Thus, the MNF transform was used in this study. The pixel purity index (PPI) was then used to find the most spectrally pure pixels in the image (Boardman et al., 1995). The PPI stipulates how many times the pixel is extreme in the simplex. The most spectrally pure pixels typically correspond to spectrally unique materials. Hence, the pixels with the highest PPI values were selected as candidate end-members as they are linearly independent in most dimensions. The final end-members were then selected by referring to the QuickBird image and the results of field survey (e.g. bare soils are mostly associated with dirt roads and cultivated areas, vegetation with homogenous canopy). This was facilitated by using the DGPS. One advantage of implementing the MNF-PPI is that it separates purer pixels from more mixed ones, thus reducing the number of pixels to be analyzed and making the separation and identification of end-members easier. Average reflectance of selected representative pixels (average of 6–20 pixels) with high PPI values that correspond to selected end-members were used in the LSMA. The scatter plot of the mean reflectance values of the end-members is shown in Fig. 2.

Four distinct end-members were identified in this study: vegetation, bare soil, non-photosynthetic materials (NPM) and water/shadow. The vegetation consists of different forest tree species such as mahogany (*Swietenia macrophylla*), narra (*Pterocarpus indicus*), acacia (*Acacia mangium*), etc. and very dense shrubs, herbs, grasses and bamboos. The bare soil end-member was taken from

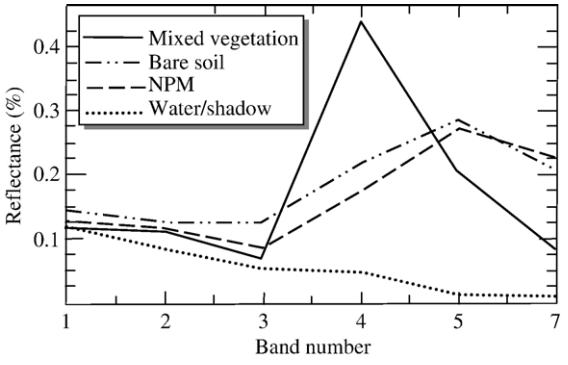

Fig. 2. Spectral curves of selected end-members.

readings in dirt roads and cultivated areas. The image was taken during the dry season, and therefore most of these areas had almost 100% exposed soil. There is only one major soil type found within the study area; "Novaliches soil" which is characterized by a reddish brown color. The soil surface cover such as dried leaves, branches, logs, rocks or gravel, along with litter represent the NPM. The candidate end-members for the NPM were extracted from open areas and abandoned cultivated lands. The final end-member, shadow, accounts for variations in illumination caused by topography and surface textures, particularly tree canopy. The shadow end-member was selected from a water body since it is assumed that both have similar spectral characteristics (Bryant, 1996).

The unmixing was constrained to ensure that the fraction of any end-member lies between 0 and 1, and the sum of fractions for each pixel is equal to 1 (Adams et al., 1986; Smith et al., 1990). The output of spectral unmixing consisted of the fraction image of each selected end-member (vegetation, bare soil, NPM and shadow/water) and a root mean square error (RMSE). The fraction images (except for shadow/water) were then used in determining the C factor values. Because shadow is not a physical component, it was removed by normalization (Adams et al., 1995; Hill et al., 1994; Smith et al., 1990). The fraction shadow/water (F_{shadow}) was removed by rescaling the three land cover fractions (vegetation, bare soil and NPM) with the normalization factor,

$$f = 1/(1 - F_{\text{shadow}}) \tag{3}$$

so that they again sum to one. This process removes only the water/shadow fraction from the image.

We then compared the percentage of vegetation (both for tree canopies and grasses), bare soil and the NPM estimated by the LSMA with the ground data. This was done to determine how well the LSMA estimated the selected end-members in the study area. The correlation was made using the average fraction of pixel values within the 2×2 pixel window and the measured data in the field.

2.5. C factor estimation

2.5.1. Linear SMA-derived C factor

Two water-related factors that cause soil erosion are rainfall and run-off. Dense forests and grasses prevent soil particles from being broken and carried downslope. Aside from vegetative cover, ground cover such as litter, slash, logs and surface rocks protect soil from the erosive forces of raindrop impact and run-off. Without cover, the rainfall impact would detach soil particles that would then be carried by running water. Kellman (1969), using small plots to measure soil erosion under various ground covers in the Philippines, reported an exponential increase in annual soil loss with decreasing ground cover. Laflen and Colvin (1981) also concluded that the greater the amount of ground cover, the lesser the soil erosion, whereas the more exposed soil or bare soil the higher the soil erosion. Utilizing this concept, we made use of the fractional abundance of bare soil and ground cover (as determined from the LSMA) to define the C factor on a pixel-by-pixel basis as follows:

$$C = \frac{F_{\text{bs}}}{1 + F_{\text{veg}} + F_{\text{NPM}}} \tag{4}$$

where, F_{bs}, F_{veg}, and F_{NPM} are the fractions of bare soil, vegetation and non-photosynthetic materials, respectively. The equation assumed that soil erosion only occurs when there are exposed soils that are subject to soil detachment by raindrop impact and surface run-off. Additionally, it was assumed that in densely vegetated areas, which could either be forest or grassland, the C value can be equal to zero. One significant result from major soil erosion studies conducted in the Philippines indicated that a good grass cover is nearly as good as dense forest and just as good as or even better than secondary forest cover in protecting the soil from erosion (Bayotlang, 1986; David, 1988; Kellman, 1969). Thus, F_{veg} in Eq. (4) could represent a grassland's or forest's vegetation. The addition of 1.0 in the denominator limits the C values from 0 to 1 with higher values indicating more exposed soil, and lower values corresponding to a high abundance of vegetation or ground cover. Using the above equation, a C factor map was generated and then compared with the C values measured in the field.

2.5.2. NDVI-derived C factor

The most common procedure for estimating C factor using the NDVI (Rouse et al., 1974) involves the use of regression equation model derived from the correlation analysis between the C factor values measured in the field and a satellite-derived NDVI (De Jong et al., 1999; De Jong and Riezebos, 1997). The NDVI expresses the difference between reflectance in the red and near-infrared (nir) bands. For a Landsat ETM, the NDVI was therefore computed utilizing band 3 (red) and band 4 (nir) as follows:

$$\text{NDVI} = \frac{\text{Band4} - \text{Band3}}{\text{Band4} + \text{Band3}} \tag{5}$$

Accordingly, a regression correlation analysis was conducted between the measured C factor taken from the 53 sampling sites and the NDVI value derived from the Landsat ETM. The average NDVI of the 2×2 pixel that matches the location of each sampling point was used. The regression equation was then employed in mapping the C factor.

2.6. Modeling soil erosion

A comparative analysis of soil erosion using the NDVI- and LSMA-derived C factor as input to soil erosion modeling was conducted employing the RUSLE model (Renard et al., 1997). The RUSLE model was chosen because of its adaptability in estimating sheet and rill erosion in tropical watersheds (Millward and Mersey, 1999). The RUSLE is an updated version that retains the original structure of the USLE. Its main advantage is that, although developed to predict soil loss under temperate conditions, its use in other regions is possible by the determination of its factors from local data (Lu et al., 2003; Lufafa et al., 2003; Millward and Mersey, 1999). Additional advantages include data requirements that are attainable under the limitations common in developing countries, and its compatibility with Geographic Information Systems (GIS) that allow for the prediction of erosion potential on a cell-by-cell basis (Millward and Mersey, 1999). The RUSLE is given as:

$$A = R \times K \times LS \times C \times P \tag{6}$$

A is the average annual soil loss predicted (t ha^{-1} y^{-1}). R is rainfall run-off erosivity factor (MJ mm ha^{-1} h^{-1} y^{-1}). This factor is measured as the product (EI) of total storm energy (E) and the maximum 30-minute intensity (I_{30}) for all storms over a long time (Renard et al., 1997). The EI parameter quantifies the effects of raindrop impact and reflects the amount and rate of run-off likely to be associated with the rain (Wischmeier and Smith, 1978). The soil erodibility factor, K (t ha h MJ^{-1} ha^{-1} mm^{-1}) reflects the ease with which the soil is detached by a splash during rainfall and/or by surface flow. This factor is related to the integrated effect of rainfall, run-off, and infiltration and accounts for the influence of soil properties on soil loss during storm events on sloping areas. The LS accounts for the effect of slope length (L) and slope gradient (S) on erosion. The C is the cover factor, which measures the effects of all interrelated cover and management variables (Renard et al., 1997). Values of C can vary from 0 for forest areas with 100% ground cover to 1 for bare soil areas (Pierce et al., 1986). The P is the support practice factor. Values for the P factor range from about 0.2 for reverse-slope bench terraces to 1 where there are no erosion control practices (Wischmeier and Smith, 1978).

The modeling of soil erosion was conducted using a raster-based approach where a square cell of 30 m was chosen to match with the spatial resolution of the Landsat ETM image. Except for the C factor which was derived using the LSMA and NDVI, all other factors (RKLSP) were determined using the procedure described in AH 703 (Renard et al., 1997) and to the works of Millward and Mersey (1999). Grids of rainfall, soil, elevation, and land cover were created using ArcInfo software. The rainfall erosivity factor for each cell was determined from the daily rainfall records in the area in which individual storm EI_{30} values were calculated according to the RUSLE methodology (Renard et al., 1997). A period of 22 years from 1980 to 2002 was used in this study. The spatial distribution of erodibility factor (K) was obtained by the interpolation of point estimates of the K factor measured in each sampling site. The soil erodibility K factor was determined using inherent soil properties following the procedure proposed by David (1988) for Philippine soils, which uses the percentage of silt, sand, and organic matter content, and the clay ratio. A digital elevation model (DEM) of the study area was generated using a linear triangular irregular network implemented in the ArcInfo software package. The LS factors were then derived using the DEM. Since there is presently no soil conservation support practices being utilized in the study area, the P factor was assigned to be equal to 1.

2.7. Soil erosion model validation

The most common method of validating the results of erosion models is through erosion surveys in which a visual estimation of erosion risk is conducted based on observed features (e.g. Cohen et al., 2005; Dwivedi et al., 1997; Metternicht and Zinck, 1998; Millward and Mersey, 1999). Previously, erosion measurements were seldom used because of the time and labor required to obtain sufficient data. In this study, we took advantage of the availability of very-high resolution remote sensing imagery to validate the output of the RUSLE model. Using a combination of a topographic map and the QuickBird image, eroded areas were located and verified in the field by precisely locating them using the DGPS. Areas representing nil, slight, moderate, high and severe soil erosion were selected and delineated in the QuickBird image. The soil erosion status was

defined according to the apparent soil erosion indicators such as the amount of vegetation, the presence of rills or gullies, whether the subsoil is exposed, the thickness of topsoil and the exposure of tree roots. For example, severe erosion was observed in areas with very sparse grass cover, exposed subsoil and where deep channels and gullies are evident. Highly eroded areas were determined by comparison with measurements from cultivated lands with exposed soil having visible rills/small channels and loss of topsoil greater than 25 cm. Grass-covered areas, with newly growing trees (i.e. mostly *Acacia auriculiformis*), a moderate loss of topsoil (less than 25 cm) and a slight exposure of tree roots were delineated as areas of moderate erosion. Slight erosion was noted in areas with no apparent soil erosion and where the loss of topsoil was insignificant. Lastly, densely vegetated forest and grass were categorized as areas with no erosion. It was assumed that due to the thickness of the vegetation cover, no soil erosion is occurring in these areas. A map of the study area depicting the five levels of soil erosion was then drawn and overlaid in the erosion map derived using the RUSLE model. The overall accuracy and kappa coefficient (Kappa) were then computed and are presented in Tables 2 and 3. The kappa coefficient was computed as follows:

$$\text{Kappa} = \frac{N\sum_{k} x_{kk} - \sum_{k} x_{k\Sigma}x_{\Sigma k}}{N^2 - \sum_{k} x_{k\Sigma}x_{\Sigma k}} \quad (7)$$

where: N is the total number of pixels in all the ground truth (reference) soil erosion classes, x_{kk} denotes the confusion matrix diagonals, $x_{k\Sigma} \times {}_{\Sigma k}$ is the product of the ground truth pixels in a class and the sum of the classified pixels in that class summed over all classes. Both the overall accuracy and kappa coefficient were determined using the image processing software ENVI 4.0 (RSI, 2004).

3. Results

Fig. 3 shows the fraction images derived using the LSMA for vegetation, bare soil, NPM and water/shadow end-members. A high abundance of each end-member is indicated by bright pixels and a low abundance by the darker pixels. The fraction images show that vegetation dominates the study area. High bare soil areas can be clearly identified which, with reference to the field data, correspond to cultivated areas and dirt roads. The fractions of non-photosynthetic materials appear to be more scattered with a relatively high abundance in open areas (abandoned cultivated lands), most of which are dried grasses. In the water/shadow fraction image, it could be observed that brighter pixels are located in areas with a high fraction of vegetation (i.e. forested areas), while darker pixels are found in open areas such as those observed in grasslands and abandoned agricultural areas. The RMSE image, representing the error between the original, mixed spectrum and the best-fit spectrum computed from the resulting end-member abundances shows a low spatial correlation (no recognizable pattern). The spatial distribution of the RMSE shows that relatively higher values (RMSE=0.007–0.013 reflectance units) can be noted in areas of bare soils and the NPM, while low values are observed in vegetated areas. The high RMSE values in the bare soil and NPM areas maybe due to the mixing or confusion of reflectance between these two end-members. However, the overall average RMSE for the whole image is still small (=0.021), thus it can be deduced that the selected end-members were valid and sufficient. The low RMSE value, however, does not guarantee that the fraction estimates are accurate. Hence, field validation was conducted to determine the accuracy of end-member estimates.

Fig. 4 shows the scatter plot correlations between the percentage of vegetation, bare soil and NPM determined with the LSMA and the field data from the 53 sampling sites. Both fractions of vegetation and bare soil demonstrated excellent correlations with r values of 0.91 and 0.89, respectively. However, a low correlation was obtained between the fraction of the NPM and the data measured in the field (r=0.50). The low correlation can be due to the confusion of reflectance among different NPM materials (not truly pure end-member). The NPM includes not only the dried leaves and branches that have fallen to the ground, but also other materials such as rocks or gravel and crop residues in abandoned cultivated areas. The problem is more complex because dead grasses, leaves and branches vary with the aging of these residues and progressively tend to be confused with other materials, such as soil when full decomposition is achieved. The separation and estimation of each of these materials may be important factors in improving the accuracy of the LSMA for use in estimating the total NPM, but the measurement and validation is impractical and not within the scope of the present study. Another reason is due to the difficulty of correlating the measured NPM with the fraction derived from the LSMA. Some measured NPM, such as decomposing leaves and branches, are taken from underneath tree canopies,

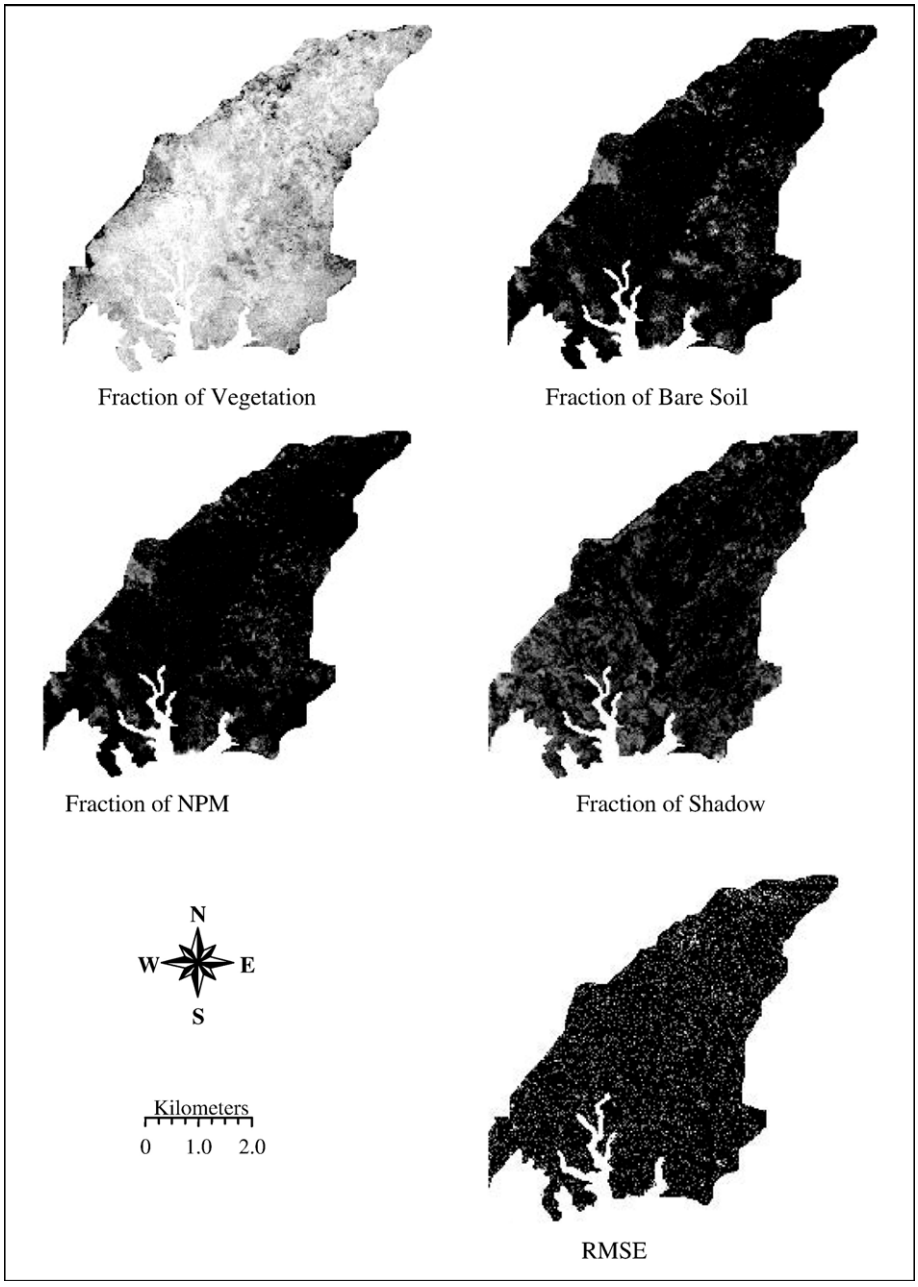

Fig. 3. Fraction and RMSE images derived from Linear Spectral Mixture Analysis of Landsat ETM. The whiter the color, the higher the proportion of end-member (and error) within the pixel.

and may not be well represented in the selected end-member.

The correlation between the field-measured *C* factor values and the NDVI was very poor ($r=0.52$); hence a quadratic function was fitted through the data. However, the fits only slightly improved the correlation with a resulting value of $r=0.64$ (Fig. 5a). This result is consistent with the results obtained by De Jong (1994) and Tweddales et al. (2000) using the correlations between the NDVI from a Landsat TM and the *C* factor. In contrast, the correlation between the LSMA-derived *C* factor and the field measured *C* factor was very good with $r=0.94$ (Fig. 5b).

The *C* factor maps derived using the LSMA and NDVI are shown in Fig. 6. The *C* factor values are shown in 14 different classes, whereby classes ranged

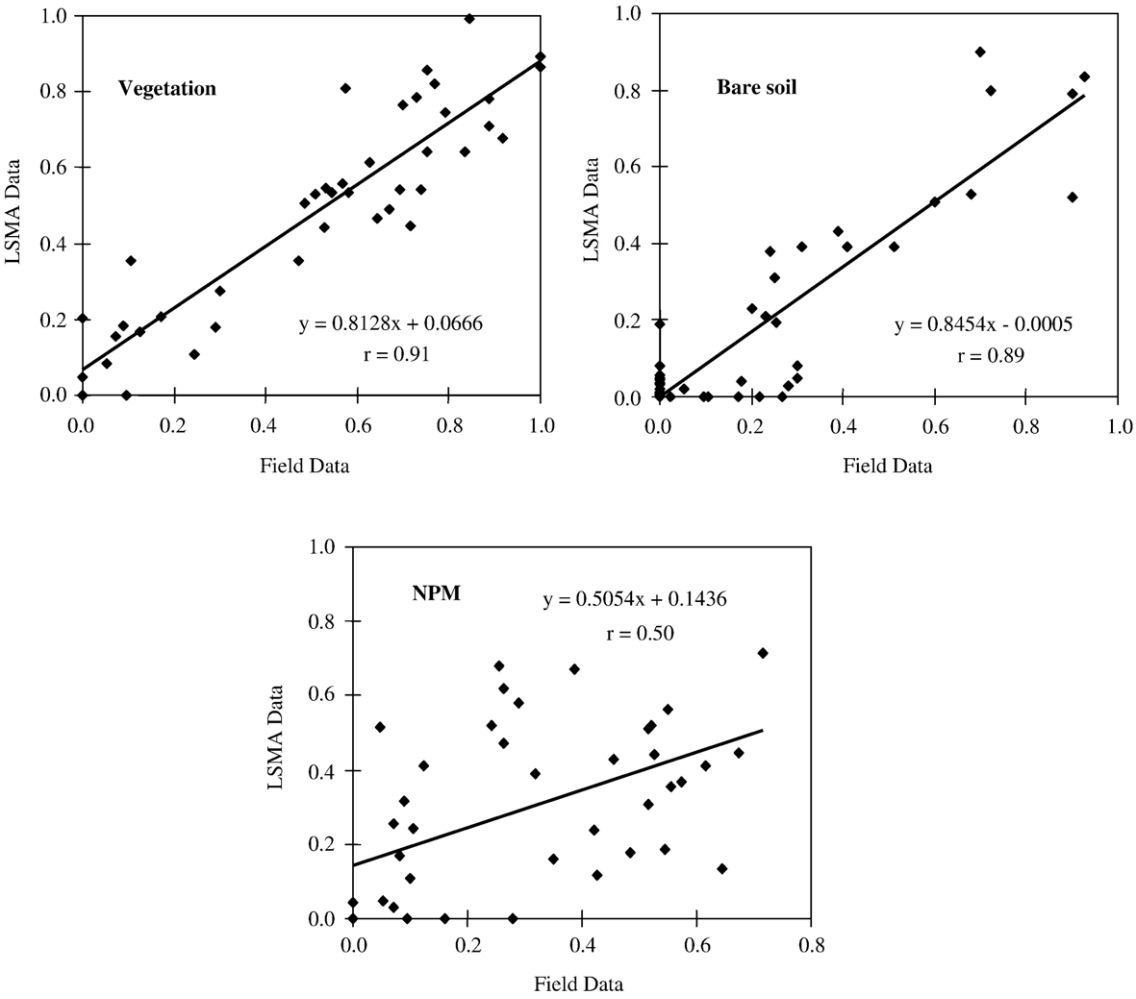

Fig. 4. Scatter plot of the LSMA-estimated fractions for vegetation, bare soil and non-photosynthetic material (NPM) against field data. Shown also are the regression equations and the correlation coefficients.

from 0 (forest) to 1 (bare soil). Notice that a clear distinction can be seen from Fig. 6a for the *C* factor values ranging from 0.0 to 0.001, which represent forested areas. The relative distribution of the *C* factor values shows that a greater portion of the study area has *C* factor values ranging from 0.05 to 0.4. In terms of land cover distribution, the classification seems satisfactory since the study area is mostly dominated by secondary growth forests and grasslands. The map also shows relatively high spatial variability that represents different cover conditions in the study area. Moreover, by comparing the field-measured *C* factor values with the tabular *C* factor values for a Philippine watershed developed by David (1988), the results can be considered good estimates.

The NDVI-derived *C* factor map, on the other hand, appears to be more homogeneous with most of *C* factor values concentrating between 0.10 and 0.40 (Fig. 6b). The highest number of pixels corresponds to *C* factor values from 0.2 to 0.3, which implies that all vegetation have been mostly classified into this category. It failed to distinguish the *C* factor for forest from other vegetation types.

3.1. Comparison and accuracy of soil erosion estimates

The quantitative output of predicted potential soil erosion using the RUSLE model was categorized into five classes, similar to the ordinal classes of soil erosion determined in the soil erosion survey (Table 1). The average natural or geologic erosion in undisturbed watershed in tropical regions is approximately 1.0 t ha^{-1} y^{-1}, hence nil erosion was defined to be within this limit. Slight erosion was set to correspond to accepted soil loss

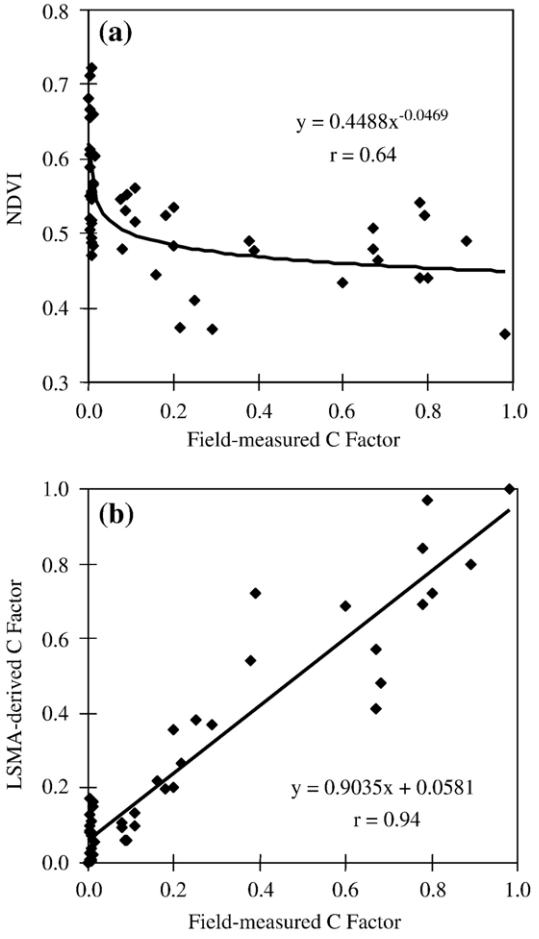

Fig. 5. Scatter plot of *C* factor measured in the field against (a) NDVI and (b) LSMA-derived *C* factor.

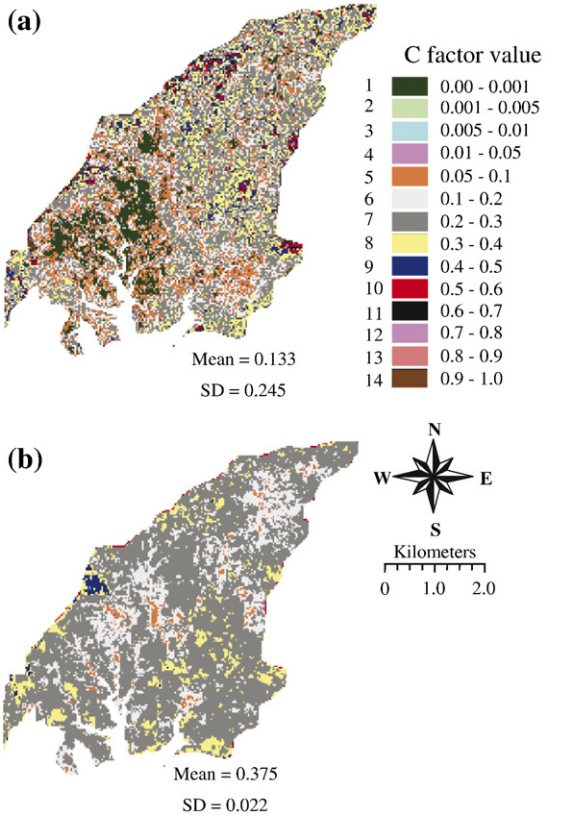

Fig. 6. *C* factor map derived using (a) LSMA and (b) NDVI method.

tolerance limit of 8 to 12 t ha^{-1} y^{-1} in the Philippines (David, 1988). The other soil erosion classes: moderate = 12 to 35 t ha^{-1} y^{-1}, high = 35 to 60 t ha^{-1} y^{-1} and severe greater than 60 t ha^{-1} y^{-1} were made based on the reported erosion rates in most soil erosion studies conducted in the Philippines. This categorization is consistent with the RUSLE model's role as a conservation management tool, where relative comparisons among land areas are more critical than assessing the absolute soil loss in a particular cell (Millward and Mersey, 1999). Comparison of the computed spatial distribution of erosion levels from both LSMA- and NDVI-derived *C* factor as inputs to the RUSLE model is shown in Fig. 7. The results of soil erosion modeling showed a significant difference in identifying the eroded areas, especially in areas with nil and severe soil erosion rates.

A comparison of areas in zones having nil, slight, moderate, high and severe soil erosion levels identified by using both methods is shown in Table 1. Using the LSMA-derived *C* factor, the estimated area with nil soil erosion is about 7% and 6% for severe erosion. This is much different from the estimated area with nil (18%) and severe erosion (19%) using the NDVI-derived *C* factor. The comparison shows that soil erosion values tend to move from high to severe erosion and slight to nil erosion when NDVI-derived *C* factor was used. This implies that the use of the NDVI-derived *C* factor may lead to an overestimation of extent of areas that require precautionary measures. On the other hand, field verification proved that locations with severe, high

Table 1
Soil erosion class and the area and proportion of each category using LSMA- and NDVI-derived *C* factors as input to RUSLE model

Soil erosion class	Numerical range (t ha^{-1} y^{-1})	LSMA (ha)	(%)	NDVI (ha)	(%)
Nil	0 to 1	157.68	7	386.73	18
Slight	1 to 12	864.54	41	710.55	33
Moderate	12 to 35	623.97	30	350.82	16
High	35 to 60	339.21	16	278.37	13
Severe	>60	128.43	6	413.64	19

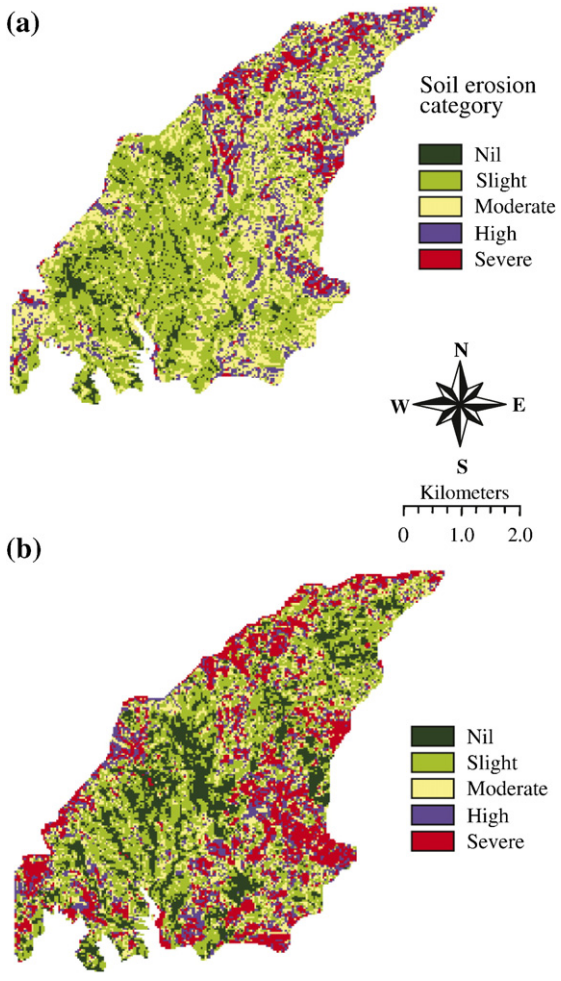

Fig. 7. RUSLE output: (a) using LSMA-derived *C* factor and (b) using NDVI-derived *C* factor as input.

and nil erosion classes were well estimated using the LSMA-derived *C* factor. Table 2 indicates that using LSMA-derived *C* factor, an overall accuracy of 70.92% and Kappa coefficient of 0.63 could be achieved in identifying the different erosion classes. This is much higher compared to the overall accuracy of 42.23% and Kappa coefficient of 0.28 using the NDVI-derived *C* factor (Table 3).

Table 2
Error matrix for soil erosion using LSMA-derived *C* factor against reference ground data

Soil erosion class	Reference data					
	Nil	Slight	Moderate	High	Severe	Total
Nil	35	2	0	1	0	38
Slight	5	50	15	1	0	71
Moderate	0	20	23	10	1	54
High	0	1	1	43	14	59
Severe	0	0	0	2	27	29
Total	40	73	39	57	42	251

Overall accuracy: 70.92.
Kappa coefficient: 0.63.

Table 3
Error matrix for soil erosion using NDVI-derived *C* factor against reference ground data

Soil erosion class	Reference data					
	Nil	Slight	Moderate	High	Severe	Total
Nil	33	10	3	6	0	52
Slight	6	20	9	8	1	44
Moderate	1	13	8	8	0	30
High	0	16	8	7	3	34
Severe	0	14	11	28	38	91
Total	40	73	39	57	42	251

Overall accuracy: 42.23.
Kappa coefficient: 0.28.

4. Discussion

The good correlation between the LSMA-derived *C* factor and the values measured in the field can be attributed to the simultaneous estimates of vegetation canopy and ground cover provided by the linear SMA. Since the *C* factor represents the protection from erosion afforded by vegetation canopy and ground cover, good estimates of these parameters are likely to produce suitable *C* factor values. One major advantage of the LSMA method is that the fraction images are directly related to the physical amount of land cover (i.e. vegetation) showing high correlations (Smith et al., 1990; Elmore et al., 2000; McGwire et al., 2000). It uncouples information from external factors such as soil brightness and color thus minimizing their influence. Hence, in terms of determining vegetation abundance, the LSMA is more accurate than the NDVI (Elmore et al., 2000). Furthermore, unlike the NDVI, which utilizes only the visible and near infrared band, the LSMA makes use of the full spectral reflectance. The LSMA can thus be used to determine not only green vegetation, but also non-photosynthetic materials, which contribute to the total ground cover protection against soil erosion.

While the NDVI is a simple and reliable measure of vegetation greenness, it does not precisely reflect the quantitative amount of protective cover against soil erosion. As documented previously, the main problems are the effect of soil reflectance (Huete et al., 1985) and the sensitivity to the vitality of the vegetation (De Jong, 1994). Vegetation under stress shows an increased reflection in the red wavelengths and a decrease in the

near infrared reflection resulting in a small NDVI value. This means that for areas having a dense cover of vegetation under stress, the NDVI will be low and, consequently, the *C* factor value will be high. The image used in this study was taken during the dry season, hence, it can be assumed that parts of the vegetation cover were under (water) stress. Moreover, vegetation in the senescent stage will have a much lower NDVI even if the vegetation cover types do not change. For soil erosion processes, the condition of vegetation cover is of minor importance. Vegetation under stress will protect the soil as well as vigorous vegetation (De Jong, 1994). In addition, the NDVI has limited capabilities to quantify the total ground cover, which includes all non-photosynthetic materials that are important in the determination of the *C* factor. Due to the absence of contrast in the reflectance between the red and the near infrared wavelengths in dry vegetation, the NDVI is not well adapted to the detection of the NPM. Thus, different indices for the detection of residue cover and/or senescent vegetation were developed such as: Brightness Index (BI) (Major et al., 1990), Cellulose Absorption Index (CAI) (Daughtry et al., 1996), Normalized Difference Index (NDI) (McNairn and Protz, 1993), Soil Adjusted Corn Residue Index (SACRI) (Biard et al., 1995), Modified Soil Adjusted Corn Residue Index (MSACRI) (Bannari et al., 1995), and Crop Residue Index Multiband (CRIM) (Biard and Baret, 1997). In this study, however, we proposed a different approach based on Spectral Mixture Analysis of Landsat ETM data to determine a fraction of the NPM.

The simplicity of deriving the NDVI from satellite images as a direct means of obtaining vegetation greenness for large areas is a primary reason for its wide use in the *C* factor determination for soil erosion assessment. Another reason could be the lack of other unsophisticated techniques to evaluate the *C* factor for regional or large-scale areas. The LSMA is simple to implement using remote sensing data and, thus, offers a better alternative. The results of the LSMA can be directly related to *C* factor values, unlike the NDVI which first needs to be correlated with field data. It is important to note, however, that the strength of the LSMA method in determining the *C* factor depends on the accuracy of end-member selection. While the LSMA results are repeatable for a given set of end-members, if the end-members are incorrect in a physical sense, then the fractional abundances, and consequently the *C* factor, will be incorrect. Nevertheless, there is available many proven methodologies and algorithms (software) that can be used to obtain appropriate end-members. This means that obtaining the necessary fractions for soil erosion analysis should not be difficult and complicated, especially for soil conservationist and watershed managers who are the primary intended users of this study, but have no advanced knowledge in satellite image processing.

One limitation of the LSMA-derived *C* factor though, is the assumption that its value is 0 under densely vegetated and good ground cover areas. This assumption implies that the overall soil erosion estimates would be underestimated in those areas. It was reported that even undisturbed forests having full, complex canopies and litter coverage still have slight erosion rates that range from 0.07 to 0.11 t ha^{-1} y^{-1} (Patric, 1976). However, taking into account that the original intent of the USLE and RUSLE was to define long-term erosion risk (Renard et al., 1997) and that the current concerns are to identify areas that need immediate rehabilitation for soil conservation purposes, the absolute values of soil erosion are not important for heavily vegetated areas.

In this study, the data used was taken during the dry season (summer of 2004). However, it should be taken into account that the *C* factor values might be different for the wet season (rainy season) in the study area. Hence, the average *C* factor for the different season must be used in the USLE or RUSLE model. The *C* values must be allocated according to the seasonal wet and dry season in the area. A multi-temporal evaluation of *C* factor is therefore needed to provide the average *C* factor to be used as input in the soil erosion model. Wischmeier and Smith (1978) suggested that the *C* factor for a year should be a weighted average based on the rainfall erosivity. For a year, a weighted *C* factor can be approximated by multiplying the *C* values by the seasonal *R* values, summing the products (CR) and dividing by the annual R. This was not considered in the present study and will be conducted in the future.

5. Conclusions

This study evaluated the suitability of the LSMA method to assess vegetation and ground cover to derive up-to-date *C* factors. This study found that the *C* factor value could be determined as a function of fractional abundance of exposed soil and ground cover derived from the LSMA. The method offers a reliable estimate of the *C* factor on a pixel-by-pixel basis, which is useful for spatial modeling of soil erosion using the RUSLE model. It should be pointed out, however, that the estimated soil erosion quantities might not be accurate as this is expressed only as the average soil erosion per year. Nevertheless, the results gave qualitative

indications of increasing soil loss with decreasing cover and accurately identified erosion areas better than the commonly used method, which is based on the NDVI. This is a significant result for watershed prioritization and soil conservation planning.

Acknowledgments

We would like to thank Mr. Marlo Mendoza, Mr. Valerio Mendoza, Mr. Glenn Paul Flores and Mr. Nemuel de Asis for their invaluable assistance during the initial data collection and fieldwork for this study. Our sincere gratitude is also accorded to the Hitachi Scholarship Foundation, Inc. (Japan) for extending financial support in the conduct of this study.

References

Adams, J.B., Smith, M.O., Johnson, P.E., 1986. Spectral mixture modeling: a new analysis of rock and soil types at the Viking Lander 1 site. Journal of Geophysical Research 91 (B8), 8098–8112.

Adams, J.B., Sabol, D.E., Kapos, V., Filho, R.A., Roberts, D.A., Smith, M.O., Gillespie, A., 1995. Classification of multispectral images based on fractions of endmembers: application to land-cover change in the Brazilian Amazon. Remote Sensing of Environment 52 (2), 137–154.

Arsenault, E., Bonn, F., 2005. Evaluation of soil erosion protective cover by crop residues using vegetation indices and Spectral Mixture Analysis of multispectral and hyperspectral data. Catena 62 (2–3), 157–172.

Bannari, A., Morin, D., Huette, A.R., Bonn, F., 1995. Modified soil adjusted crop residue index (MSACRI): a new index for mapping crop residue. http://ieeexplore.ieee.org/iel5/6913/18664/00860296.pdf (accessed April 2, 2007).

Baver, L.D., 1956. Soil Physics, third ed. John Wiley & Sons Inc., New York.

Bayotlang, E.L., 1986. Evaluation of Erosivity, Erodibility and Crop Management Factors of the Universal Soil Loss Equation. PhD Thesis, University of the Philippines Los Banos, Laguna, Philippines.

Beasley, D.B., Huggins, L.F., Monke, E.J., 1980. ANSWERS: a model for watershed planning. Transactions of the American Society of Agricultural Engineers 23 (4), 938–944.

Biard, F., Baret, F., 1997. Crop residue estimation using multiband reflectance. Remote Sensing of Environment 59 (3), 530–536.

Biard, F., Bannari, A., Bonn, F., 1995. SACRI (Soil Adjusted Corn Residue Index): un indice utilisant le proche et le moyen infrarouge pour la de´tection des re´sidus de cultures de maý¨s. Proc. 17th Canadian Symposium on Remote Sensing, Saskatoon, Canada, June 17–21, pp. 417–423.

Boardman, J.W., Kruse, F.A., Green, R.O., 1995. Mapping target signatures via partial unmixing of AVIRIS data. Fifth JPL Airborne Earth Science Workshop, Pasadena California, January 23–26, vol. 95(1). JPL Publication, pp. 23–26.

Bryant, R.G., 1996. Validated linear mixture modelling of Landsat TM data for mapping evaporite minerals on a playa surface: methods and applications. International Journal of Remote Sensing 17 (2), 315–330.

Cartagena, D.F., 2004. Remotely Sensed Land Cover Parameter Extraction for Watershed Erosion Modeling. MSc. Thesis, International Institute for Geo-information Science and Earth Observation, Enschede, The Netherlands, ITC publications.

Cihlar, J., 1987. A methodology for mapping and monitoring cropland soil erosion. Canadian Journal of Soil Science 67 (3), 433–444.

Cohen, M.J., Shepherd, K.D., Walsh, M.G., 2005. Empirical reformulation of the universal soil loss equation for erosion risk assessment in a tropical watershed. Geoderma 124 (3–4), 235–252.

Daughtry, C.S.T., McMurtrey III, J.E., Chappelle, E.W., Hunter, W.J., Steiner, J.L., 1996. Measuring crop residue cover using remote sensing techniques. Theoretical and Applied Climatology 54 (1–2), 17–26.

David, W.P., 1988. Soil and water conservation planning: policy issues and recommendations. Journal of Philippine Development 15 (26), 47–84.

Dwivedi, R.S., Ravi Sankar, T., Venkataratnam, L., Karale, R.L., Gawande, S.P., Seshagin Rao, K.V., Senchaudhary, S., Bhaumik, K.R., Mukharjee, K.K., 1997. The inventory and monitoring of eroded lands using remote sensing data. International Journal of Remote Sensing 18 (1), 107–119.

De Jong, S.M., 1994. Derivation of vegetative variables from a Landsat TM image for modelling soil erosion. Earth Surface Processes and Landforms 19 (2), 165–178.

De Jong, S.M., Riezebos, H.T., 1997. SEMMED: a distributed approach to soil erosion modelling. In: Spiteri, A. (Ed.), Remote Sensing '96: Integrated Applications for Risk Assessment and Disaster Prevention for the Mediterranean. Balkema, Rotterdam, pp. 199–204.

De Jong, S.M., Paracchini, M.L., Bertolo, F., Folving, S., Megier, J., De Roo, A.P.J., 1999. Regional assessment of soil erosion using the distributed model SEMMED and remotely sensed data. Catena 37 (3–4), 291–308.

Dissmeyer, G.E., Foster, G.R., 1981. Estimating the cover-management factor (C) in the Universal Soil Loss Equation for forest conditions. Journal of Soil and Water Conservation 36 (4), 235–240.

Elmore, A.J., Mustard, J.F., Manning, S.J., Lobell, D.B., 2000. Quantifying vegetation change in semiarid environment: precision and accuracy of Spectral Mixture Analysis and the Normalized Difference Vegetation Index. Remote Sensing of Environment 73 (1), 87–102.

Elwell, H.A., Stocking, M.A., 1976. Vegetal cover to estimate soil erosion hazard in Rhodesia. Geoderma 15 (1), 61–70.

Folly, A., Bronsveld, M.C., Clavaux, M., 1996. A knowledge-based approach for C-factor mapping in Spain using Landsat TM and GIS. International Journal of Remote Sensing 17 (12), 2401–2415.

Ganey, J.L., Block, W.M., 1994. A comparison of two techniques for measuring canopy closure. Western Journal of Applied Forestry 9 (1), 21–23.

Garcia, M., Ustin, S.L., 2001. Detection of interannual vegetation responses to climatic variability using AVIRIS data in a Coastal Savanna in California. IEEE Transactions on Geoscience and Remote Sensing 39 (7), 1480–1490.

Gertner, G., Wang, G., Fang, S., Anderson, A.B., 2002. Mapping and uncertainty of predictions based on multiple primary variables from joint co-simulation with Landsat TM image and polynomial regression. Remote Sensing of Environment 83 (3), 498–510.

Gilabert, M.A., Garcia-Haro, F.J., Melia, J., 2000. A mixture modeling approach to estimate vegetation parameters for heterogeneous canopies in remote sensing. Remote Sensing of Environment 72 (3), 328–345.

Hazarika, M.K., Honda, K., 2001. Estimation of soil erosion using remote sensing and GIS: its valuation and economic implications on agricultural production. In: Stott, D.E., Mohtar, R.H., Steinhardt, G.C. (Eds.), Sustaining the Global Farm. Purdue University and USDA-ARS National Soil Erosion Research Laboratory, pp. 1090–1093.

Hill, J., Mehl, W., Altherr, M., 1994. Land degradation and soil erosion mapping in Mediterranean ecosystems. In: Hill, J., Megier, H. (Eds.), Imaging Spectrometry — a Tool for Environment Observations. Dordrecht, Kulwer Academic Publishers, pp. 237–260.

Huang, C., Wylie, B., Yang, L., Homer, C., Zylstra, G., 2002. Derivation of a tasselled cap transformation based on Landsat 7 at-satellite reflectance. International Journal of Remote Sensing 23 (8), 1741–1748.

Huete, A.R., Jackson, R.D., Post, D.F., 1985. Spectral response of a plant canopy with different soil backgrounds. Remote Sensing of Environment 17 (1), 37–53.

Juergens, C., Fander, M., 1993. Soil erosion assessment by means of Landsat-TM and ancillary digital data in relation to water quality. Soil Technology 6 (3), 215–223.

Kellman, M.C., 1969. Some environmental components of shifting cultivation in upland Mindanao. Journal of Tropical Geography 28 (1), 40–56.

Kerdiles, H., Grondona, M.O., 1995. NOAA-AVHRR NDVI decomposition and subpixel classification using linear mixing in the Argentinean Pampa. International Journal of Remote Sensing 16 (7), 1303–1325.

Laflen, J.M., Colvin, T.S., 1981. Effect of crop residue on soil loss from continuous row cropping. Transactions of the American Society of Agricultural Engineers 24 (3), 605–609.

Lin, C.-Y., Lin, W.-T., Chou, W.-C., 2002. Soil erosion prediction and sediment yield estimation: the Taiwan experience. Soil and Tillage Research 68 (2), 143–152.

Lin, W.-T., Lin, C.-Y., Chou, W.-C., 2006. Assessment of vegetation recovery and soil erosion at landslides caused by a catastrophic earthquake: a case study in Central Taiwan. Ecological Engineering 28 (1), 79–89.

Lu, H., Prosser, I.P., Moran, C.J., Gallant, J.C., Priestly, G., Stevenson, J.G., 2003. Predicting sheetwash and rill erosion over the Australian continent. Australian Journal of Soil Research 41 (6), 1037–1062.

Lufafa, A., Tenywa, M.M., Isabirye, M., Majaliwa, M.J.G., Woomer, P.L., 2003. Prediction of soil erosion in a Lake Victoria basin catchment using a GIS-based universal soil loss model. Agricultural Systems 76 (3), 883–894.

Major, D.J., Baret, F., Guyot, G., 1990. A ratio vegetation index adjusted for soil brightness. International Journal of Remote Sensing 11 (5), 727–740.

McGwire, K., Minor, T., Fenstermaker, L., 2000. Hyperspectral mixture modeling for quantifying sparse vegetation cover in arid environments. Remote Sensing of Environment 72 (3), 360–374.

McNairn, H., Protz, R., 1993. Mapping corn residue cover on agricultural fields in Oxford county, Ontario, using Thematic Mapper. Canadian Journal of Remote Sensing 19 (2), 152–159.

Metternicht, G.I., Zinck, J.A., 1998. Evaluating the information content of JERS-1 SAR and Landsat TM data for discrimination of soil erosion features. ISPRS Journal of Photogrammetry and Remote Sensing 53 (3), 143–153.

Millward, A.A., Mersey, J.E., 1999. Adapting the RUSLE to model soil erosion potential in a mountainous tropical watershed. Catena 38 (2), 109–129.

Morgan, R.P.C., 1995. Soil Erosion and Conservation, second ed. Longman Group Limited, Essex, UK.

Morgan, R.P.C., Morgan, D.D.V., Finney, H.J., 1984. A predictive model for the assessment of soil erosion risk. Journal of Agricultural Engineering Research 30 (1), 245–253.

Morrison, J.E., Huang, C., Lightle, D.T., Daughtry, C.S.T., 1993. Residue measurement techniques. Journal of Soil and Water Conservation 48 (11), 479–483.

Myneni, R.B., Maggion, S., Iaquinta, J., Privette, J.L., Gobron, N., Pinty, B., Kimes, D.S., Verstraete, M.M., Williams, D.L., 1995. Optical remote sensing of vegetation: modeling, caveats, and algorithms. Remote Sensing of Environment 51 (1), 169–188.

Najmoddini, N., 2003. Assessment of Erosion and Sediment Yield Processes Using Remote Sensing and GIS: A Case Study in Rose Chai Sub-catchment of Orumieh Basin, W.Azarbaijan, MSc. Thesis, International Institute for Geo-information Science and Earth Observation, Enschede, The Netherlands, ITC publications.

NSERL, 1995. WEPP User Summary. National Soil Erosion Research Laboratory, US Department of Agriculture. http://topsoil.nserl.purdue.edu/nserlweb/weppmain/docs/readme.htm (accessed March 30, 2007).

Oki, K., Oguma, H., Sugita, M., 2002. Subpixel classification of alder trees using multitemporal Landsat Thematic Mapper imagery. Photogrammetric Engineering and Remote Sensing 68 (1), 77–82.

Paningbatan, E.P., 2001. Geographic Information System-assisted dynamic modeling of soil erosion and hydrologic processes at a watershed scale. Philippine Agricultural Scientist 84 (4), 388–393.

Paringit, E.C., Nadaoka, K., 2003. Sediment yield modelling for small agricultural catchments: land-cover parameterization based on remote sensing data analysis. Hydrological Processes 17 (9), 1845–1866.

Patric, J.H., 1976. Soil erosion in the eastern forest. Journal of Forestry 129 (10), 671–677.

Peterson, S.H., Stow, D.A., 2003. Using multiple image endmember Spectral Mixture Analysis to study chaparral regrowth in Southern California. International Journal of Remote Sensing 24 (22), 4481–4504.

Pierce, F.J., Larson, W.E., Dowdy, R.H., 1986. Soil Conservation: An Assessment of the National Resources Inventory, vol. 2. National Academy Press, Washington, D.C.

Renard, K.G., Foster, G.R., Weesies, G.A., McCool, D.K., Yoder, D.C., 1997. Predicting Soil Erosion by Water: A Guide to Conservation Planning with the Revised Universal Soil Loss Equation (RUSLE). US Department of Agriculture, Agricultural Handbook Number, vol. 703. Government Printing Office, Washington, D.C.

Research Systems Inc. (RSI), 2004. ENVI 4.0 User's Guide. Pearl East Circle, Boulder, Colorado, USA.

Roberts, D.A., Smith, M.O., Adams, J.B., 1993. Green vegetation, nonphotosynthetic vegetation and soils in AVIRIS data. Remote Sensing of Environment 44 (2–3), 255–269.

Rouse, J.W., Hass, R.W., Schell, J.A., Deering, D.W., Harlan, J.C., 1974. Monitoring the Vernal Advancement and Retrogradation (Greenwave Effect) of Natural Vegetation. NASA/GSFCT Type III Final report. Greenbelt, Maryland, USA.

Settle, J.J., Drake, N.A., 1993. Linear mixing and the estimation of ground cover proportions. International Journal of Remote Sensing 14 (6), 1159–1177.

Shoshany, M., Svoray, T., 2002. Multidate adaptive unmixing and its application to analysis of ecosystem transitions along a climatic gradient. Remote Sensing of Environment 82 (1), 5–20.

Small, C., 2003. High spatial resolution Spectral Mixture Analysis of urban reflectance. Remote Sensing of Environment 88 (1–2), 170–186.

Smith, M.O., Ustin, S.L., Adams, J.B., Gillespie, A.R., 1990. Vegetation in deserts: I. a regional measure of abundance from multispectral images. Remote Sensing of Environment 31 (1), 1–26.

Stephens, P.R., Cihlar, J., 1982. Mapping erosion in New Zealand and Canada. In: Johannsen, C.J., Sanders, J.L. (Eds.), Remote Sensing and Resource Management. Soil Conservation Society of America, Ankeny, IA, pp. 232–242.

Symeonakis, E., Drake, N., 2004. Monitoring desertification and land degradation over sub-Saharan Africa. International Journal of Remote Sensing 25 (3), 573–592.

Tompkins, S., Mustard, J.F., Pieters, C.M., Forsyth, D.W., 1997. Optimization of endmembers for Spectral Mixture Analysis. Remote Sensing of Environment 59 (3), 472–489.

Tweddales, S.C., Eschlaeger, C.R., Seybold, W.F., 2000. An Improved Method for Spatial Extrapolation of Vegetative Cover Estimates (USLE/RUSLE *C* factor) using LCTA and Remotely Sensed Imagery. USAEC report No. SFIM-AEC-EQ-TR-200011, ERDC/CERL TR-00-7, US Army of Engineer Research and Development Center, CERL, Champaign, Illinois.

Van der Knijff, J., Jone, R.J.A., Montanarella, L., 2002. Soil erosion risk assessment in Italy. European Soil Bureau, Joint Research Center of European Commission. EUR 19022EN.

Van der Meer, F., 1995. Spectral unmixing of Landsat Thematic Mapper data. International Journal of Remote Sensing 16 (16), 3189–3194.

Van der Meer, F., De Jong, S.M., 2000. Improving the results of spectral unmixing of Landsat Thematic Mapper imagery by enhancing the orthogonality of end-members. International Journal of Remote Sensing 21 (15), 2781–2797.

Wang, G., Wente, S., Gertner, G.Z., Anderson, A., 2002. Improvement in mapping vegetation cover factor for the universal soil loss equation by geostatistical methods with Landsat Thematic Mapper images. International Journal of Remote Sensing 23 (18), 3649–3667.

Wang, G., Gertner, G., Fang, S., Anderson, A.B., 2003. Mapping multiple variables for predicting soil loss by geostatistical methods with TM images and a slope map. Photogrammetric Engineering and Remote Sensing 69 (8), 889–898.

Wischmeier, W.H., Smith, D.D., 1978. Predicting Rainfall Erosion Losses: A Guide to Conservation Planning. US Department of Agriculture, Agricultural Handbook Number, vol. 537. Government Printing Office, Washington, D.C.

Wu, C., Murray, A.T., 2003. Estimating impervious surface distribution by Spectral Mixture Analysis. Remote Sensing of Environment 84 (4), 493–505.

Xiao, J., Moody, A., 2005. A comparison of methods for estimating fractional green vegetation cover within a desert-to-upland transition zone in central New Mexico, USA. Remote Sensing of Environment 98 (2–3), 237–250.